Available online at BCREC website: https://bcrec.id

Bulletin of Chemical Reaction Engineering & Catalysis, 18 (3) 2023, 362-374

Research Article

Green Synthesis of Cr-PTC-HIna Metal Organic Frameworks (MOFs) and Its Application in Methylene Blue Photocatalytic Degradation

Nur Mahrunisa[1], Adawiah Adawiah[2,*], Isalmi Aziz[1], Agustino Zulys[3]

[1]Department of Chemistry, Faculty of Science and Technology, UIN Syarif Hidayatullah Jakarta, Jl. Ir. H. Juanda No. 95 Ciputat Tangerang Selatan 15412, Indonesia.
[2]Integrated Laboratory Centre, Faculty of Science and Technology UIN Syarif Hidayatullah Jakarta, Jl. Ir. H. Juanda No. 95 Ciputat Tangerang Selatan 15412, Indonesia.
[3]Department of Chemistry, Faculty of Mathematics and Natural Sciences, University of Indonesia, Jl. Lingkar Kampus Raya, Pondok Cina, Beji, Depok, Jawa Barat 16424, Indonesia.

Received: 18th June 2023; Revised: 13th August 2023; Accepted: 14th August 2023
Available online: 18th August 2023; Published regularly: October 2023

Abstract

Metal Organic Framework (MOF) is a material that serves as a photocatalyst for decomposing methylene blue pollutant. MOF can be constructed using several kinds of synthetic methods. This study aims to determine the alternative efficient and eco-friendly synthesis method of isonicotinic acid-modulated chromium perylene 3,4,9,10-tetracharboxylate MOF (Cr-PTC-HIna) using solvothermal, hydrothermal, sonochemical, and mechanochemical methods. FTIR analysis revealed that Cr-PTC-HIna was successfully fabricated only by solvothermal, hydrothermal, and sonochemical methods, yielding 40.68%, 44.27%, and 46.50%. Cr-PTC-HIna-ST, Cr-PTC-HIna-HT, and Cr-PTC-HIna-SC have band gap energies of 2.02, 2.02, and 1.98 eV, respectively. Cr-PTC-HIna-HT and Cr-PTC-HIna-SC with irregular shapes form agglomerations. Cr-PTC-HIna-SC had the highest surface area, pore volume, and pore size of 92.76 $m^2.g^{-1}$, 0.3947$cm^3.g^{-1}$, and 142.74 nm, respectively. Cr-PTC-HIna-SC has the highest percentage of methylene blue decolorization through adsorption of 61.843% and photocatalytic degradation of 25.635%. Sonochemical and hydrothermal showed potential as more eco-friendly methods than solvothermal in synthesizing Cr-PTC-HIna MOF.

Keywords: Hydrothermal; mechanochemical; MOF Cr-PTC-HIna; solvothermal; sonochemical

How to Cite: N. Mahrunisa, A. Adawiah, I. Aziz, A. Zulys (2023). Green Synthesis of Cr-PTC-HIna Metal Organic Frameworks (MOFs) and Its Application in Methylene Blue Photocatalytic Degradation. *Bulletin of Chemical Reaction Engineering & Catalysis*, 18(3), 362-374 (doi: 10.9767/bcrec.18885)

Permalink/DOI: https://doi.org/10.9767/bcrec.18885

1. Introduction

Methylene blue is a heterocyclic aromatic compound that widely applied as a dye for cellulose fibers, silk, wool, leather, and paper [1]. However, because only five percent of methylene blue's solution is employed in its application, the remaining ninety-five percent will be disposed of as aquatic waste [2]. Methylene blue is persistent and difficult to degrade naturally, hence special treatment is required to remove harmful methylene blue waste from the aquatic environment.

Various methods, both conventional and modern, have been extensively applied to remove organic dye pollutants from wastewater, including chemical oxidation, coagulation, ad-

* Corresponding Author.
Email: adawiah@uinjkt.ac.id (A. Adawiah);
Telp: +62-812-8347-2535

sorption, ion exchange, and photocatalysis [3,4]. Photocatalysis is considered as the most efficient and cost-effective approach for degrading organic dye pollutants into an environmentally benign product [5]. The photocatalysis process generates free radicals capable of completely degrading dye contaminants. Photocatalysis is environmentally friendly since it does not need the additional chemicals such as ozone to degrade contaminants, can be operated at room temperature and can degrade toxic organic pollutants into CO_2 and H_2O compounds [6–8].

The materials that may serve as a photocatalyst is semiconductor like metal oxide such as Bi_2O_3 and metal-organic frameworks like La-PTC (MOF) [9–14]. MOF is a three-dimensional organic-inorganic hybrid material designed from metal oxides or metal ions are bonded to each other in the presence of organic linkers [15,16]. Organic linkers in MOFs act as light traps and activate metal oxide, allowing them to act as semiconductors [17]. The advantages of MOF than the other photocatalyst materials are large surface area and porous size, which may be modified by adjusting the molecular size of the organic linker and/or changing the functional groups on the linker [18].

MOFs can be synthesized using a number of techniques, including solvothermal, hydrothermal, sonochemical, and mechanochemical. MOF's crystals can be generated immediately from solution applying hydrothermal and solvothermal processes, particle size and shape can be modified by using different starting materials and reaction conditions [19]. Lee *et al*. [20] successfully synthesized MOF zeolitic imidazolate frameworks-8 using the solvothermal method with a surface area of 1370 m^2g^{-1}, particle size of 150-200 nm, pore volume of 0.51 cm^3g^{-1}, and yield of 60%. Meanwhile, Butova *et al*. [21] synthesized ZIF-8 using the hydrothermal method and a tiny amount of TEA to form crystals.

Many researchers have applied green chemistry concept in recent decades, which deals with the synthesis of materials using more ecologically benign methods. Mohammed and Errayes stated that green chemistry is a concept related with chemical procedures that reduce or eliminate the use of hazardous raw materials in the fabrication of a product [22]. Green chemistry is concerned with synthesis methods that contribute to the sustainability of chemical processes, energy savings, lower toxicity of reagents and end products, less environmental and human health damage, reduced risk of global warming, and rational utilization of natural resources and agricultural waste. Glowniak *et al*. [23] reported that green synthesis can be accomplished by lowering the amount of solvent and energy needed.

Sonochemical method is known to be more environmentally friendly than solvothermal and hydrothermal approaches since they utilize ultrasonic radiation in crystal synthesis. The sonochemical approach also has the advantage of being able to break down massive crystal aggregates into nanometer-sized ones, consuming less energy and low temperatures, yielding more, and allowing for intermediate reactions [19]. Liu *et al*. [24] reported that the ultrasonically approach is environmentally benign because the chemical reaction occurs at ambient conditions (room temperature and atmospheric pressure) and the reaction time required is less than that of conventional methods. Lee *et al*. [20] effectively synthesized ZIF-8 using sonochemical and a deprotonating agent in the form of triethylamine that formed crystals with a crystalline structure.

The mechanochemical approach is yet another green synthesis method. Mechanochemical is a green synthesis process since the product formation reaction occurs quickly between solid precursors under solvent-free conditions (or with the addition of a tiny amount of solvent). Milling may decrease synthesis time and energy consumption since the thermal energy released during the operation is sufficient to activate chemical reactions without heating [19]. Mechanochemical procedures are particularly eco-friendly because they do not use any solvents, the obtained products have greater yields, and the formation of MOF crystals may be accomplished in a short time (10 to 60 min) [25]. Lee *et al*. [20] effectively synthesized ZIF-8 using a mechanochemical technique and ammonium salts as deprotonating agents, obtaining crystals with a surface area of 1256 m^2g^{-1}, pore size of 3-15 nm, pore volume of 0.64 cm^3g^{-1}, and an 82% yield.

High yield and purity, the use of solvents and minimal energy, and subsequent photocatalytic activity are significant factors in determining the MOF synthesis method. Adawiah *et al*. [26] employed a solvothermal technique to synthesize isonicotinic acid-modulated MOF Cr-PTC-HIna, which can degrade methylene blue 95.40% after 180 min of exposure to a 250-watt mercury lamp.

Following to the literature review, the synthesis of isonicotinic acid-modulated chromium perylene 3,4,9,10-tetracharboxylate MOF (Cr-

PTC-HIna) by applying more environmentally friendly methods such as hydrothermal, sonochemical, and mechanochemical and utilized it for methylene blue photocatalytic degradation have never been carried out. Therefore, this work aims to synthesize Cr-PTC-HIna MOF based photocatalyst through solvothermal, hydrothermal, sonochemical, and mechanochemical methods to determine the most efficient green synthesis method in producing this MOF crystals both in percent yield, physico-chemical characteristics and photocatalytic activity in methylene blue degradation.

2. Materials and Methods

2.1 Materials

The materials used in this work were purchased from chemical distributor in Indonesia, and used without futher purification. These materials are $CrCl_3.6H_2O$ grade emsure (Merck, p.a.), perylene-3,4,9,10-tetracarboxylic dianhydride (Merck, p.a.), NaOH grade emsure (Merck, p.a.), *N,N*-dimethyl formamide grade emsure (Merck, p.a.), isonicotinic acid (Merck, p.a.), ethanol technical grade, KBr grade emsure (Merck, p.a.), methylene blue (Merck, p.a.), and distilled water.

2.2 Preparation of Sodium perylene-3,4,9,10-tetracarboxylate (Na_4PTC) from Perylene-3,4,9,10-tetracarboxylic dianhydride (PTCDA) [23]

Perylene-3,4,9,10-tetracarboxylic dianhydride (PTCDA) (0.5 g) and NaOH (0.356 g) were dissolved in 50 mL of distilled water and magnetically stirred at room temperature for an hour. The greenish-yellow filtrate was subsequently added with excessive ethanol to produce a yellow precipitate. The yellow precipitate of Na_4PTC was filtered and washed with ethanol until the pH was neutral, then dried at room temperature overnight. Fourier Transform Infrared (FTIR) was used to characterize the obtained Na_4PTC powder.

2.3 Synthesis of Cr-PTC-HIna MOF

2.3.1 Solvothermal Method [26]

The chromium(III) chloride hexahydrate ($CrCl_3.6H_2O$) (1 mmol, 0.2660 g), Na_4PTC (0.5 mmol, 0.2580 g), and isonicotinic acid (0.5 mmol, 0.0615 g) were mixed and dissolved in a DMF (5 mL) and distilled water (25 mL) solvent mixture. The suspension was frequently stirred using the magnetic stirrer at 300 rpm for an hour. The suspension was transferred to Teflon-line stainless steel autoclave, and then heated at 170 °C for 24 h. The obtained precipitate was filtered and purified with distilled water. The brown precipitate was dried overnight at 70 °C. The final product was designed as Cr-PTC-HIna-ST.

2.3.2 Hydrothermal Method

The hydrothermal method in this study was carried out the same as the solvothermal method, except that in the hydrothermal method the use of organic solvent (DMF) was eliminated. $CrCl_3.6H_2O$ salt (1 mmol, 0.2660 g), Na_4PTC (0.5 mmol, 0.2580 g), and isonicotinic acid (0.5 mmol, 0.0615 g) were mixed and diluted in 30 mL of distilled water. The mixture was frequently stirred using the magnetic stirrer at 300 rpm for an hour. The mixed solution was transferred to Teflon-line stainless steel autoclave, and then heated at 170 °C for 24 h. The obtained precipitate was filtered and purified with distilled water. The red brown precipitate was dried overnight at 70 °C. The final product was designed as Cr-PTC-HIna-HT.

2.3.3 Sonochemical Method

Chromium(III) chloride hexahydrate ($CrCl_3.6H_2O$) (1 mmol, 0.2660 g), Na_4PTC (0.5 mmol, 0.2580 g), and isonicotinic acid (0.5 mmol, 0.0615 g) were combined as well as dissolved in a mixture of DMF (5 mL) and distilled water (25 mL). For 1 h, the mixture was stirred constantly with a magnetic stirrer at 300 rpm. The solution was transferred to a capped Erlenmeyer flask and placed in an ultrasonicator. The sonication process took 180 min at 25 °C, with a frequency of 60 Hz and a voltage of 240 V. The precipitate formed in the sonication mixture was filtered and washed with distilled water until the filtrate was clear. The precipitate was then dried at 70 °C overnight. The final product was designed as Cr-PTC-HIna-SC.

2.3.4 Mechanochemical Method

The chromium(III) chloride hexahydrate ($CrCl_3.6H_2O$) (1 mmol, 0.266 g), Na_4PTC (0.5 mmol, 0.258 g), and isonicotinic acid (0.5 mmol, 0.0615 g) were mixed and mashed for 45 min at room temperature using a mortar and pestle. The mixture had been dried at 70 °C overnight. Cr-PTC-HIna-MC was the product's code.

2.4 Characterization of Cr-PTC-HIna

The four Cr-PTC-HIna were characterized using XRD (Rigaku Miniflex XRD) with Cu-Kα

radiation (λ=1.5418 Å) with a 2θ range of 3°-90° and a scan rate of 2 °/min. The crystal size of Cr-PTC-HIna was calculated using the Debye Scherrer equation. The functional groups of Cr-PTC-HIna were determined using a FTIR spectrophotometer (Prestige 21 Spectrophotometer) in the wavenumber region 400-4000 cm^{-1} with a spectral resolution of 4 cm^{-1} by using KBr powder as the blank. Band gap energy of Cr-PTC-HIna was measured using an UV-Vis DRS spectrophotometer (Agilent Cary 60 UV-Vis) with a blank of $BaSO_4$ powder, and calculated it using the Kubelka Munk-Tauc Plot equation. The morphology and distribution of elements of Cr-PTC-HIna were investigated using SEM-EDX (Jeol JSM 6510 La) at a voltage of 25 kV. The surface area, pore volume, and pore size of Cr-PTC-HIna were assessed using a surface area and porosity analyzer (Micromeritics Tristar II Plus Surface Area & Porosity Analyser) after a 3 h degassing process at 150 °C.

2.5 Photocatalytic Activity of Cr-PTC-HIna Analysis

Cr-PTC-HIna (0.025 g) was disperse in 50 mL of 50 ppm methylene blue and stirred at 300 rpm for 2 h, while illuminated with a 250-watt mercury lamp. Furthermore, the suspension was centrifuged at 6000 rpm for 10 min. The absorbance of methylene blue was determined using a UV-Vis spectrophotometer at 665 nm. The decolorization percentage of methylene blue was calculated using equation (1).

$$\%decolorization = \frac{A_0 - A_t}{A_0} \times 100\% \quad (1)$$

where, %decolorization is the methylene blue removal percentage, A_0 is the initial absorbance of methylene blue and A_t is the absorption of methylene blue at time.

3. Results and Discussion

3.1 Cr-PTC-HIna MOF

The Cr-PTC-HIna was synthesized using solvothermal, hydrothermal, sonochemical, and mechanochemical methods to discover the most efficient and eco-friendly method for producing these MOFs for methylene blue degradation application. The employment of hydrothermal, sonochemical, and mechanochemical processes provides various environmental benefits due to the application of green chemistry concepts. Figure 1 shows the physical properties of Cr-PTC-HIna MOF obtained through the four techniques.

Figure 1 demonstrates the physical properties of Cr-PTC-HIna created by each method, namely, the colors produced in MOFs made by hydrothermal (a), solvothermal (b), sonochemical (c), and mechanochemical (d) processes are bright red, brick red, brown, and blackish brown, respectively. These discrepancies occur due to the influence of various treatments utilized during the synthesis process, such as energy and solvents. This study's solvothermal and hydrothermal approaches possess identical process steps, with the difference being the solvent used; the hydrothermal method only uses distilled water solvent, and the solvothermal method uses a mixture of distilled water and DMF solvent.

The percent yields of Cr-PTC-HIna-ST, Cr-PTC-HIna-HT, Cr-PTC-HIna-SC, and Cr-PTC-HIna-MC were 40.68%, 44.27%, 46.5%, and 49.23%, respectively. It is clear that the MOFs synthesized by hydrothermal, sonochemical, and mechanochemical methods have a higher percent yield than solvothermal. MOF produced using the mechanochemical method has the highest yield since there are impurities due to the lack of a washing step, which influences the amount of product formed. Meanwhile, because Na_4PTC and $CrCl_3.6H_2O$ dissolve better in aqueous solvents than organic solvents such as DMF, the hydrothermal process obtained a higher percent yield than the solvothermal method. The greater solubility accelerates in the nucleation process by enhancing the frequency of particle collisions, which increases the number of metal ions and organic linkers that bind and form MOFs.

Sonochemical methods may create more MOFs with a higher percentage yield than hydrothermal and solvothermal methods because the use of ultrasonic radiation provides significantly more kinetic energy than conventional methods, reducing crystallization time and leading to the formation of more MOF's crystals. Because of the acoustic cavitation process, ultrasonic irradiation provides shorten the crystallization time [27]. This method reaches

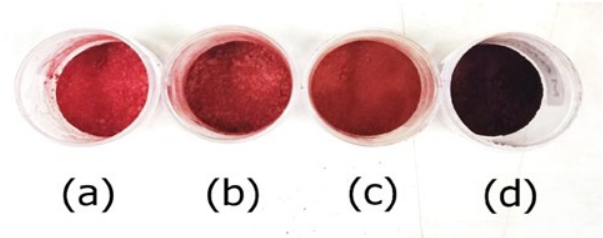

Figure 1. Physical characteristic of (a) Cr-PTC-HIna-HT; (b) Cr-PTC-HIna-ST; (c) Cr-PTC-HIna-SC; (d) Cr-PTC-HIna-MC.

temperatures of more than 5000 K and pressures of more than 20 MPa, with heating and cooling rates of more than 107 K/s, increasing the reaction kinetics of product synthesis [28]. The acoustic cavitation process also increased the frequency of particle collisions as well as direct interaction between particles and irradiation waves, lowering activation energy [29]. According to Pourebrahimi and Kazemeini, MIL-101(Cr) generated by sonochemical approach has a greater crystallization rate than solvothermal synthesis, resulting in a higher yield [30].

3.2 Functional Group of Cr-PTC-HIna MOF

The FTIR spectra of Cr-PTC-HIna-ST, Cr-PTC-HIna-HT, and Cr-PTC-HIna-SC MOF are similar to those of the previously synthesized Cr-PTC-HIna MOF [26] (Figure 2). The FTIR spectra of Cr-PTC-HIna-ST, Cr-PTC-HIna-HT, and Cr-PTC-HIna-SC revealed the existence of asymmetric and symmetric stretching vibration absorption bands of C=O (1800-1600 cm^{-1}) and C−O (1300-900 cm^{-1}) groups that were not present in the Na_4PTC spectrum (Figure 2). Furthermore, the absence of the OH group absorption band of carboxylic acid at 3500-2800 cm^{-1} suggests that the COO− group on isonicotinic acid has bonded with Cr^{3+} to form Cr-COO (Figure 2). The asymmetric (1650-1540 cm^{-1}) and symmetric (1450-1360 cm^{-1}) O−C=O groups in Na_4PTC shifted in the Cr-PTC-HIna spectra, confirming the existence of PTC linkers coordinated on Cr in the MOF structure. Metal oxide bond (Cr−O) vibrations can be seen at 800-400 cm^{-1}. Aromatic ring features were discovered in the form of 1,2,3,4-tetrasubstituted C−H out of plane bending vibrations (675-900 cm^{-1}) and C=C out of plane vibrations (675-900 cm^{-1}). Meanwhile, the IR spectrum of the mechanochemically synthesized MOF did not demonstrate the synthesis of Cr-PTC-HIna since there were no symmetric absorption bands of C=O, C−O, and Cr−O bonds.

3.3 The XRD Spectrum of Cr-PTC-HIna MOF

The XRD spectrum of the Cr-PTC-HIna-HT and Cr-PTC-HIna-ST MOFs in this study and the Cr-PTC-HIna synthesized in previous studies are identical [22]. The XRD spectrum (Figure 3) of MOF Cr-PTC-HIna-SC resembled but differed significantly from that of MOF Cr-PTC-HIna-ST. Although Cr-PTC-HIna-SC has a different diffraction pattern from Cr-PTC-HIna-ST, the sonochemical method can still produce Cr-PTC-HIna MOFs. It is supported by the FTIR analysis results, which show identical FTIR spectra between Cr-PTC-HIna-ST and Cr-PTC-HIna-SC. The difference in the XRD spectrum of Cr-PTC-HIna-SC indicates that Cr-PTC-HIna-SC has a different crystal structure from Cr-PTC-HIna-ST. It also occurs in anatase and rutile TiO_2; namely, anatase forms diffraction peaks at 25° (101) and 53.8° (211), while rutile forms diffraction peaks at 36.7° (110) and 62.7° (002) [31]. This difference occurs due to the difference in energy used during the crystal formation process.

A shift in the diffraction peak of 2θ values, which corresponds to changes in the product's crystallinity and crystal size, supported the difference. Figure 3 shows that Cr-PTC-HIna-MC failed to obtain MOF because the XRD spectrum was difference with the previous Cr-PTC-HIna. The XRD spectrum of Cr-PTC-HIna-MC

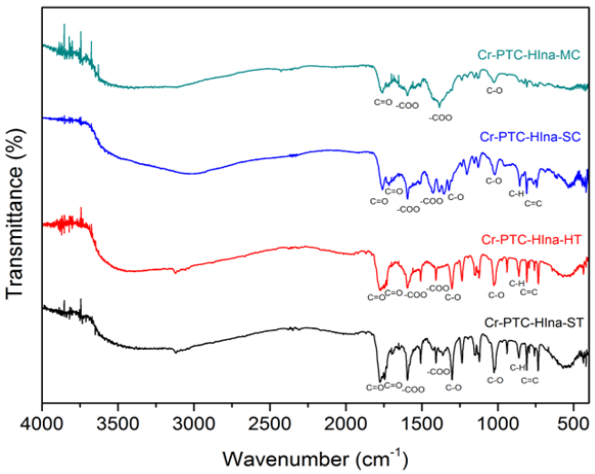

Figure 2. The FTIR spectrum of Cr-PTC-HIna-ST, Cr-PTC-HIna-HT, Cr-PTC-HIna-SC, and Cr-PTC-HIna-MC.

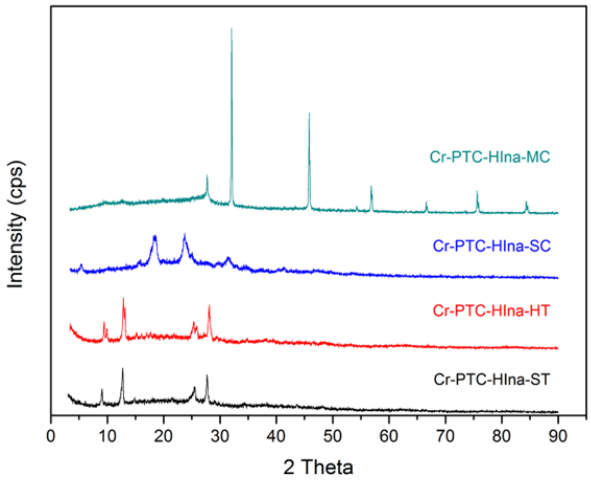

Figure 3. The XRD spectrum of Cr-PTC-HIna-ST, Cr-PTC-HIna-HT, Cr-PTC-HIna-SC, and Cr-PTC-HIna-MC.

demonstrates the presence of Cr_3O_4 and Na_2O compounds, as shown by the presence of the greatest peak in 2θ of 32.7° and 46.23°, respectively (According to the VESTA analytical results (supplementary file), and JCPDS File No. 12-559).

The crystallinity of Cr-PTC-HIna-ST and Cr-PTC-HIna-HT is greater than Cr-PTC-HIna-SC, as shown in Figure 3. Strong and narrow peaks suggest the MOFs are completely pure crystallin [32]. The difference in crystallinity is due to the synthesis time and temperature affected the crystallization process of MOF. Kareem and Abd Alrubaye explained that the more intensive the crystallization process and temperature used in the solvothermal synthesis of MOF-199, the higher the crystallinity of MOF-199 [33]. Pressures, on the other hand, promote a shift in diffraction angle and a decrease in peak intensity in Cr-PTC-HIna-SC, confirming crystal defects in nanoparticle materials [34].

The poor crystallinity of Cr-PTC-HIna-SC is also related to the use of water solvents, which inhibit crystal formation and result in a less crystalline MOF framework. Because anions and solvents form strong hydrogen bonds through the solvation effect, protic polar solvents like water increase activation energy [35]. DMF, on the other hand, may reduce activation energy by releasing anions toward covalently coupled cations [36]. Zhang *et al.* [37] observed that Cu-BTC could not be successfully synthesized using aqueous solvents under ultrasonic irradiation because water hinders the formation of coordination bonds between the carboxyl groups of BTC and Cu. Israr *et al.* [36] reported that the synthesis of Ni-BTC with DMF solvent under ultrasonic irradiation produced the MOF framework within 2 h, however the synthesis with water/ethanol solvent under the same conditions did not.

The crystal size of the three Cr-PTC-HIna MOFs was calculated using the Debye Scherrer equation. The crystal size of Cr-PTC-HIna-ST, Cr-PTC-HIna-HT, and Cr-PTC-HIna-SC were 36.92 nm, 18.97 nm, and 7.48 nm, respectively. The Cr-PTC-HIna-ST and Cr-PTC-HIna-HT were synthesized at particularly high temperatures, resulting in a larger crystal size than the

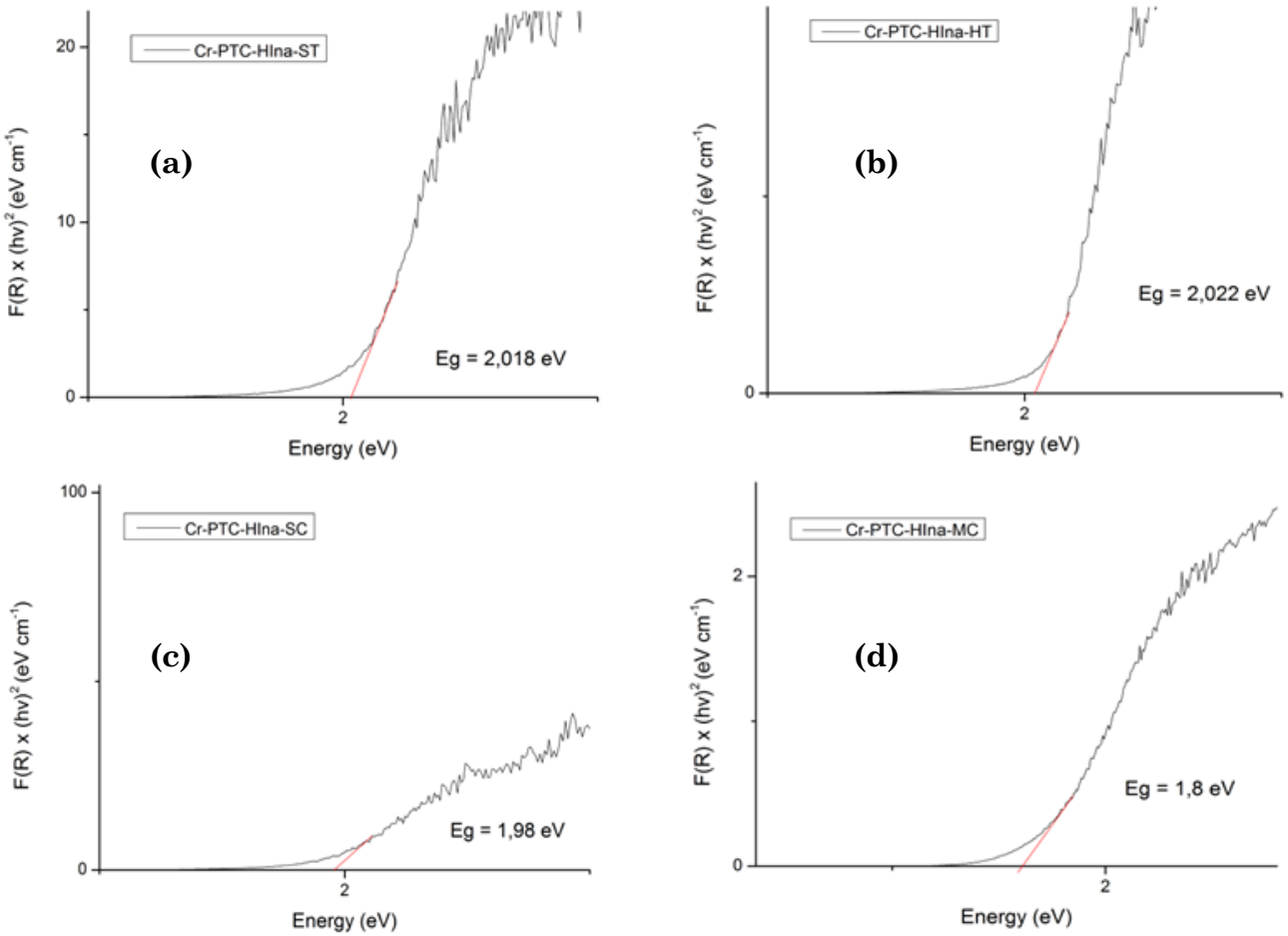

Figure 4. Bandgap energy of (a) Cr-PTC-HIna-ST; (b) Cr-PTC-HIna-HT; (c) Cr-PTC-HIna-SC; and (d) Cr-PTC-HIna-MC.

Cr-PTC-HIna-SC. Sharma *et al*. [38] stated that higher temperatures facilitate the growth of larger crystals. This is proven by Cr-PTC-HIna-SC's low crystallinity, which indicates that the diffraction peaks have risen, implying that the crystal size is significantly smaller than Cr-PTC-HIna-ST and Cr-PTC-HIna-HT. Pereira *et al*. [39] employed a sonochemical method to produce a larger diffraction peak and a smaller crystal size of 21.11.6 nm than Barros *et al*. [40] who used a traditional method to produce a crystal size of 72.1 nm.

3.4 Bandgap Energy of Cr-PTC-HIna MOF

The band gap energy was examined to determine the responsiveness of Cr-PTC-HIna MOF to visible light. This study made use of a mercury lamp, which emits 17% UV light and 83% visible light. The band gap energy was measured using the Kubelka-Munk equation and the Tauc plot (Figure 4).

The band gap energy of Cr-PTC-HIna-ST, Cr-PTC-HIna-HT, Cr-PTC-HIna-SC, and Cr-PTC-HIna-MC is 2.018, 2.022, 1.980, and 1.800 eV, respectively, resulting in maximum light absorption at 615, 613, 626, and 688 nm. The four Cr-PTC-HIna MOFs absorb visible light, allowing them to serve as visible-light responsive photocatalysts.

3.5 Cr-PTC-HIna Morphology and Elemental Composition

Figure 5 shows the morphologies of Cr-PTC-HIna-ST, Cr-PTC-HIna-HT, and Cr-PTC-HIna-SC, and Cr-PTC-HIna-MC. Cr-PTC-HIna-ST, Cr-PTC-HIna-HT, and Cr-PTC-HIna-SC are all MOFs having irregular structures. As shown in Figure 5, the purity of Cr-PTC-HIna-ST is lower than that of Cr-PTC-HIna-HT. Pollutants in the shape of transverse rods suggest this. Impurities in MOF crystals originate by an excess of DMF solvent that is not completely removed during the washing or drying procedures. Cr-PTC-HIna-MC has a different morphology from Cr-PTC-HIna, Cr-PTC-HIna-HT, and Cr-PTC-HIna-SC. It indicates that the mechanochemical method did not successfully obtain MOF.

The SEM-EDX results of all materials reveal the presence of different impurities such as Ca, Zr, Cu, and Zn (Table 1). It can be caused by the drying process in the oven, where the Cr-PTC-HIna MOF lacks relief material like aluminum foil, allowing a number oven pollutants adhere to the MOF surface.

Figure 5 depicts the formation of agglomerations by the Cr-PTC-HIna-HT and Cr-PTC-HIna-SC MOFs. Agglomeration occurs because both techniques have a faster crystal growth rate than Cr-PTC-HIna-ST. The rapid crystal growth rate in tiny materials causes agglomeration. According to Liu *et al*. [41] agglomeration is generated by extended ultrasonic irradiation and a rise in particle impact frequency. Zarekarizi and Morsali [42] reported TMU-69 has a smaller particle size as the sonication time increases, and using ultrasonic irradiation for more than 60 min causes the formation of aggregates as the TMU-69 particles agglomerate. The decrease in crystallinity in Cr-PTC-HIna-SC MOF is due to agglomeration.

The particle size of the Cr-PTC-HIna-SC is smaller and more uniform than the other two MOFs. It is due to ultrasonic vibrations accelerate the dissociation rate of the precursor, leading the reaction to become more homogeneous, resulting in the formation of smaller and more uniform MOF particles [43]. It also prov-

Table 1. SEM-EDX Analysis Data of Cr-PTC-HIna MOFs.

No.	Sample	Element	Concentration (%w/w)
1.	Cr-PTC-HIna-ST	C	55.94
		O	34.12
		Ca	0.08
		Cr	9.86
2.	Cr-PTC-HIna-HT	C	56.84
		O	35.44
		Cl	0.20
		Cr	7.13
		Zr	0.39
3.	Cr-PTC-HIna-SC	C	58.64
		O	35.17
		Cr	5.37
		Cu	0.41
		Zn	0.41

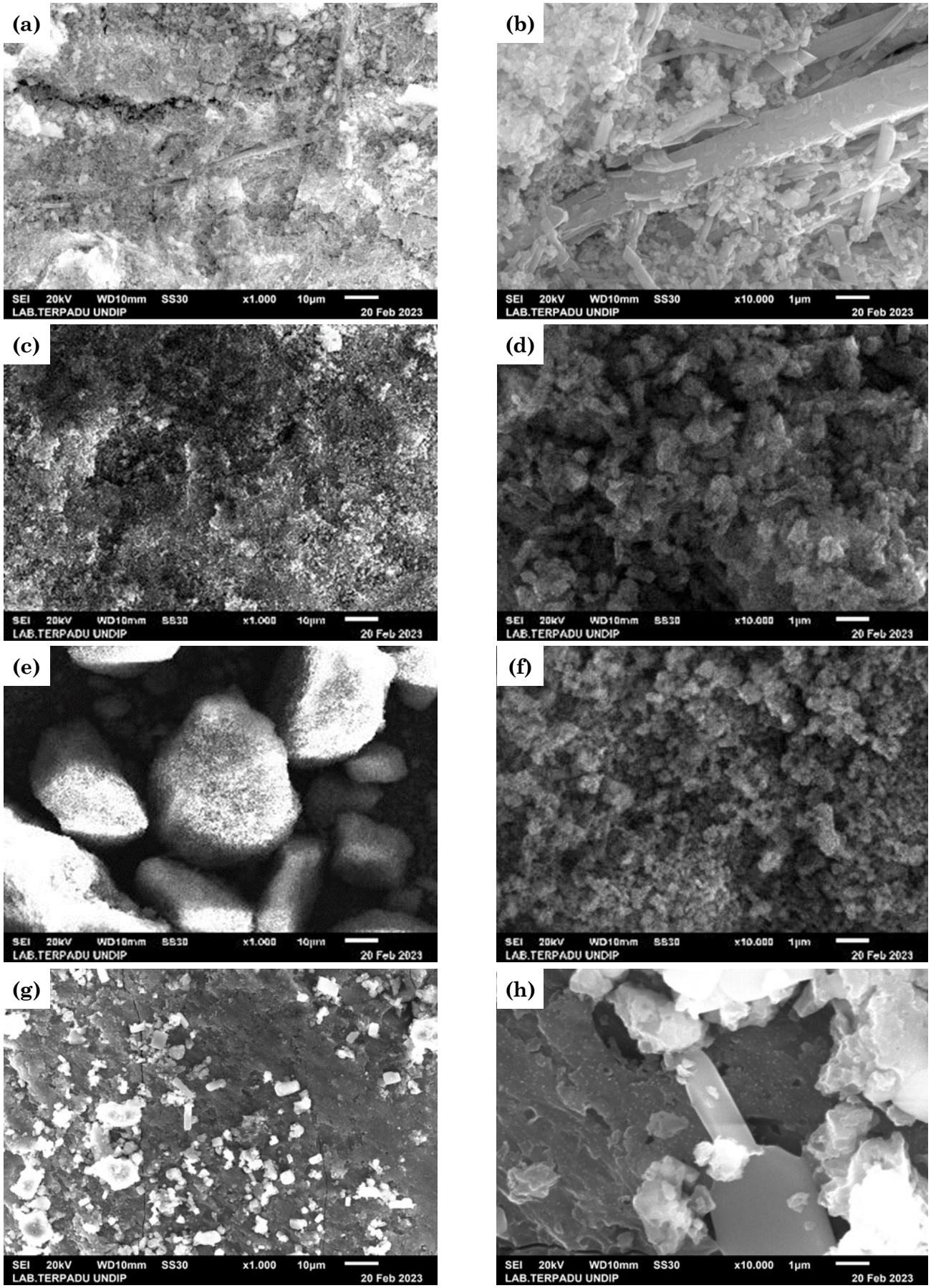

Figure 5. MOF morphology with magnificent 1000x and 10000x of Cr-PTC-HIna-ST (a-b); Cr-PTC-HIna-HT (c-d); Cr-PTC-HIna-SC (e-f); Cr-PTC-HIna-MC (g-h).

en by Pereira *et al*. [39] who synthesized Zn-MOF that formed agglomerations with smaller, regular, and uniform particle size. Furthermore, Cu-BTC synthesized by Abbasi and Rizvandi via sonochemical method for an hour ultrasonic irradiation has smaller particle size (80 nm) than conventional method synthesis by Barros *et al*. for 24 h at 80 °C (140 nm) [44,40].

3.6 Surface Area, Pore Volume and Pore Diameter of Cr-PTC-HIna

The surface area measurement in Cr-PTC-HIna MOFs was calculated using the BET equation. The BET method is applied because it can accurately assess the porosity and surface area of porous materials based on the principle of absorption of gas molecular species on the surface of the measured solids [45].

The Cr-PTC-HIna-SC MOF had the highest surface area, pore volume, and pore diameter size of the three methods, as shown in Table 2. The presence of crystal defects in the crystal structure of the MOF contributes to its tremendous surface area. The XRD spectrum (Figure 3) supports it. The number of crystal defect sites rises as a result of ultrasonic radiation. Ultrasonic radiation increases crystal formation, preventing the exchange of protonated modulators and PTC molecules on Cr during synthesis. Yu *et al*. [46] reported that sonochemically synthesized S-MOF-545 has more defect sites than solvothermally synthesized C-MOF-545. The presence of defects in the crystal improves the surface area and pore volume of S-MOF-545 over C-MOF-545 [46].

Furthermore, the relatively small particle size of Cr-PTC-HIna-SC allows its surface area to be larger than other MOFs (Figure 5(f)). Pourebrahimi and Kazemeini observed that sonochemically synthesized MIL-101 Cr has a larger BET surface area than solvothermally designed MIL-101 Cr [30]. Furthermore, HKUST-1 obtained through sonochemical methods has a larger surface area than solvothermal [43].

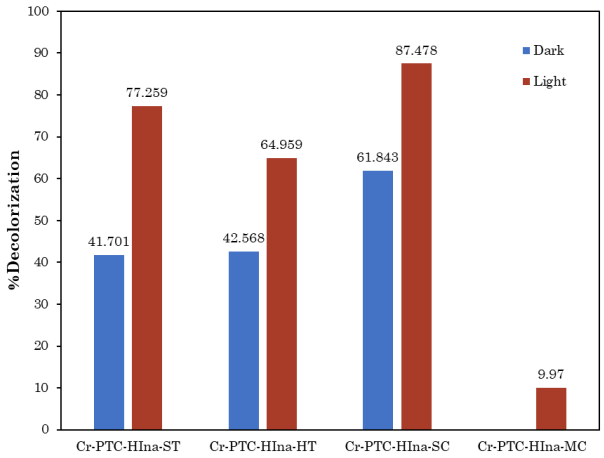

Figure 6. Decolorization percentage of methylene blue by Cr-PTC-HIna-ST, Cr-PTC-HIna-HT, Cr-PTC-HIna-SC, and Cr-PTC-HIna-MC.

3.7 Photocatalytic Activity of Cr-PTC-HIna

The four materials were investigated for photocatalytic activity against methylene blue decolorization in both dark and light conditions. The percentage of methylene blue decolorization accomplished by the adsorption process was measured in the dark condition. As a porous material, it can remove methylene blue via adsorption and photocatalytic degradation. Figure 6 presents the percentage of methylene blue decolorization under both conditions.

Figure 6 illustrates the percentages of methylene blue decolorization in the dark for Cr-PTC-HIna-ST, Cr-PTC-HIna-HT, Cr-PTC-HIna-SC, and Cr-PTC-HIna-MC, which are 41.701%, 42.568%, 61.843%, and 0.0%, respectively. The three MOFs most likely decolored methylene blue via adsorption. This adsorption approach employs π-π, and electrostatic interaction. The positively charged sulfur and nitrogen atoms of methylene blue interact with the negatively charged bonds of the Cr-PTC-HIna benzene ring via electrostatic interactions. Furthermore, π-π interactions occur between the aromatic rings' bonds in methylene blue and perylene Cr-PTC-HIna [26].

Figure 6 additionally reveals that Cr-PTC-HIna-SC has a higher adsorption ability than Cr-PTC-HIna-ST and Cr-PTC-HIna-HT. Cr-PTC-HIna-SC has a large surface area, volume, and pore diameter size, all of which contribute to its high adsorption capacity. The higher the surface area of the MOF, the more

Table 2. Surface area analyzer measurement data of Cr-PTC-HIna.

Sample	Surface Area (m^2/g)	Pore Volume (cm^3/g)	Pore Diameter (Å)
Cr-PTC-HIna-ST	59.44	0.1187	81.610
Cr-PTC-HIna-HT	35.24	0.1000	37.851
Cr-PTC-HIna-SC	92.76	0.3947	142.738
Cr-PTC-HIna-MC	6.43	0.0137	33.525

active sites with which methylene blue molecules interact. Furthermore, the excessive size and volume of the pores will improve methylene blue molecule absorption. Meanwhile, the Cr-PTC-HIna-MC has no adsorption ability since the proportion of MB decolorization is zero. It could be due to the surface area, as well as the small diameter and volume pore; there are no functional groups or atoms capable of reacting with methylene blue.

Figure 6 shows that the percentage of methylene blue decolorization by the Cr-PTC-HIna-ST, Cr-PTC-HIna-HT, and Cr-PTC-HIna-SC is higher in light than in dark conditions. It implies that the three MOFs have significant photocatalytic activity in the methylene blue decolorization process. When exposed to light, MOFs behave as photocatalysts. Organic linkers act as antennas, capturing light from natural or artificial light sources and using it to activate metal sites [47]. Organic linkers have delocalized orbitals due to conjugated π bonds, which transfer the electron charge towards the metal-oxo group at the initial step of the photo-redox process [48]. The XRD spectra (Figure 3) of Cr-PTC-HIna-MC is similar with metal oxide compounds, so that Cr-PTC-HIna-MC was unsuccessful to produce appropriate MOF. However, the resulting product may be useful as a photocatalyst. It is confirmed by the test results in light condition (Figure 6). The photocatalytic activity of Cr-PTC-HIna-MC is relatively poor due to the limited surface area and porosity (Table 2). Although the band gap energy of Cr-PTC-HIna-MC is sufficient for photocatalysis of methylene blue, the small surface area diminishes the number of active sites for the electron photoexcitation process.

The photocatalytic activity of the Cr-PTC-HIna-ST was higher than the Cr-PTC-HIna-HT and Cr-PTC-HIna-SC, with percentage decolorization increases of 35.34%, 22.40%, and 25.64%, respectively. However, Cr-PTC-HIna-SC provides the highest removal efficiency of 87.478% methylene blue via a combination of adsorption and photocatalytic processes than Cr-PTC-HIna-ST and Cr-PTC-HIna-HT (Figure 6). It is due to its high surface area, large pore size, and pore volume.

Cr-PTC-HIna-ST exhibits higher photocatalytic activity than Cr-PTC-HIna-HT due to its larger surface area, pore volume, and pore size. The increased surface area suggests that the number of active sites accessible for the excitation of electron-hole pairs (e^-/h^+) and redox activities, as well as the number of reactive radicals generated for the methylene blue photodegradation process, is rising [49]. Larger material porosity accelerate photocatalytic degradation of dye pollutants by trapping considerable amounts of pollutants before they are degraded by the photocatalyst [50]. On the other hand, Cr-PTC-HIna-ST has larger crystal size and higher crystallinity, resulting in greater photodecomposition rate of organic compounds than Cr-PTC-HIna-HT.

However, the photocatalytic activity of Cr-PTC-HIna-SC is lower than Cr-PTC-HIna-ST because the pore size of Cr-PTC-HIna-SC is too large, allowing methylene blue to enter and trapped in the pores of Cr-PTC-HIna, making the methylene blue difficult to desorb towards the photocatalyst surface, resulting in a decrease in the photocatalytic degradation reaction. Furthermore, as the amount of methylene blue molecules absorbed increases, the layer of dye molecules covering the photocatalyst surface thickens. It reduces the intensity of light contacting the surface of the photocatalyst due to methylene blue molecule absorption, hence decreasing the electron excitation process and the radical species that play a role in the methylene blue degradation process.

Crystal defects in the Cr-PTC-HIna-SC hindered photocatalytic activity. Yu *et al*. [46] reported that the sonochemical method produces materials with more defect sites than conventional methods. The low crystallinity of the Cr-PTC-HIna-SC (Figure 3) affirms it, suggesting that the Cr-PTC-HIna is less crystalline due to the presence of excess crystal defects. Surface crystal defects trap electron charges within the material's framework, inhibiting photoexcitation. Furthermore, as the number of crystal defects increases, so does the rate of electron-hole pair recombination, resulting in fewer hydroxyl radical molecules. Xiao and Jiang [51] explained that a small number of crystal defects could decrease electron-hole pairs recombination in MOFs.

4. Conclusions

Solvothermal, hydrothermal, and sonochemical methods could be utilized for obtaining MOF Cr-PTC-HIna. The solvothermal method obtained MOF Cr-PTC-HIna with the maximum photocatalytic activity for methylene blue degradation, with a 35.34% decolorization enhancement via photocatalytic degradation. Sonochemical and hydrothermal method could be more eco-friendly alternative ways than solvothermal for producing Cr-PTC-HIna MOF.

Acknowledgment

The authors would like to express their gratitude to UIN Syarif Hidayatullah Jakarta for financial support under contract number B-301/LP2MPUSLITPEN/TL.02/2023.

CRediT Author Statement

Adawiah was in responsible for conceptualization, validation, resources, data curation, writing, review, and editing; N. Mahrunissa was in duty of formal analysis, investigation, data gathering, and draft preparation. I. Aziz oversaw writing, reviewing, and editing. A. Zulys discussed on research, resources, and writing. All authors read the manuscript promptly approved it for future publish.

References

[1] Bayomie, O.S., Kandeel, H., Shoeib, T., Yang, H., Youssef, N., El-Sayed, M.M.H. (2020). Novel approach for effective removal of methylene blue dye from water using fava bean peel waste. *Scientific Reports*, 10, 7824. DOI: 10.1038/s41598-020-64727-5.

[2] Yagub, M.T., Sen, T.K., Afroze, S., Ang, H.M. (2014). Dye and its removal from aqueous solution by adsorption: A review. *Advances in Colloid and Interface Science,* 209, 172–184. DOI: 10.1016/j.cis.2014.04.002.

[3] Cheng, Y.J., Wang, R., Wang, S., Xi, X.J., Ma, L.F., Zang, S.Q. (2018). Encapsulating $[Mo_3S_{13}]^{2-}$ clusters in cationic covalent organic frameworks: enhancing stability and recyclability by converting a homogeneous photocatalyst to a heterogeneous photocatalyst. *Chemical Communications*, 54, 13563–13566. DOI: 10.1039/C8CC07784C.

[4] Velegraki, G., Miao, J., Drivas, C., Liu, B., Kennou, S., Armatas, G. (2018). Fabrication of 3D mesoporous networks of assembled CoO nanoparticles for efficient photocatalytic reduction of aqueous Cr(VI). *Applied Catalysis B: Environmental,* 221, 635–644. DOI: 10.1016/j.apcatb.2017.09.064.

[5] Zhao, N., Sun, F., Zhang, N., Zhu, G. (2017). Novel pyrene-based anionic metal-organic framework for efficient organic dye elimination. *Crystal Growth & Design*, 17, 2453–2457. DOI: 10.1021/acs.cgd.6b01864.

[6] Kumar, P.S., Selvakumar, M., Babu, S.G., Karuthapandian, S. (2016). Veteran cupric oxide with new morphology and modified bandgap for superior photocatalytic activity against different kinds of organic contaminants (acidic, azo and triphenylmethane dyes). *Materials Research Bulletin,* 83, 522–533. DOI: 10.1016/j.materresbull.2016.06.043.

[7] Mahmoodi, N.M. (2015). Manganese ferrite nanoparticle: synthesis, characterization, and photocatalytic dye degradation ability. *Desalination and Water Treatment*, 53, 84–90. DOI: 10.1080/19443994.2013.834519.

[8] Nageri, M., Kalarivalappil, V., Vijayan, B.K., Kumar, V. (2016). Titania nanotube arrays surface-modified with ZnO for enhanced photocatalytic applications. *Materials Research Bulletin,* 77, 35–40. DOI: 10.1016/j.materresbull.2016.01.020.

[9] Astuti, Y., Musthafa, F., Arnelli, A., Nurhasanah, I. (2022). French fries-like bismuth oxide: physicochemical properties, electrical conductivity and photocatalytic activity. *Bulletin of Chemical Reaction Engineering & Catalysis,* 17(1), 146–156. DOI: 10.9767/bcrec.17.1.12554.146-156.

[10] Astuti, Y., Amri, D., Widodo, D.S., Widiyandari, H., Balgis, B., Ogi, T. (2020). Effect of fuels on the physicochemical properties and photocatalytic activity of bismuth oxide, synthesized using solution combustion method. *International Journal of Technology,* 11(1), 26–36. DOI: 10.14716/ijtech.v11i1.3342.

[11] Astuti, Y., Andianingrum, R., Arnelli, A., Haris, A., Darmawan, A. (2020). The role of $H_2C_2O_4$ and Na_2CO_3 as precipitating agents on the physichochemical properties and photocatalytic activity of bismuth oxide. *Open Chemistry,* 18, 129–137. DOI: 10.1515/chem-2020-0013.

[12] Habisreutinger, S.N., Schmidt-Mende, L., Stolarczyk, J.K. (2013). Photocatalytic reduction of CO_2 on TiO_2 and other semiconductors. *Angewandte Chemie International Edition*, 52, 7372–7408. DOI: 10.1002/anie.201207199.

[13] Silva, C.G., Corma, A., García, H. (2010). Metal–organic frameworks as semiconductors. *Journal of Materials Chemistry,* 20, 3141–3156. DOI: 10.1039/B924937K.

[14] Zulys, A., Adawiah, A., Gunlazuardi, J., Yudhi, M.D.L. (2021). Light-harvesting metal-organic frameworks (MOFs) La-PTC for photocatalytic dyes degradation. *Bulletin of Chemical Reaction Engineering & Catalysis,* 16, 170–178. DOI: 10.9767/bcrec.16.1.10309.170-178.

[15] Araya, T., Jia, M., Yang, J., Zhao, P., Cai, K., Ma, W., Huang, Y. (2017). Resin modified MIL-53 (Fe) MOF for improvement of photocatalytic performance. *Applied Catalysis B: Environmental*, 203, 768–777. DOI: 10.1016/j.apcatb.2016.10.072.

[16] Zhao, C., Jiang, H., Liang, Q., Zhou, M., Zhang, Y., Li, Z., Xu, S. (2020). NH_2-UiO-66 with heterogeneous pores assists zinc indium sulfide in accelerating the photocatalytic H_2 evolution under visible-light irradiation. *Solar Energy,* 207, 599–608. DOI: 10.1016/j.solener.2020.07.005.

[17] Foster, M.E., Azoulay, J.D., Wong, B.M., Allendorf, M.D. (2014). Novel metal–organic framework linkers for light harvesting applications. *Chemical Science,* 5, 2081–2090. DOI: 10.1039/C4SC00333K.

[18] Furukawa, H., Cordova, K.E., O'Keeffe, M., Yaghi, O.M. (2013). The chemistry and applications of metal-organic frameworks. *Science,* 341, 974–986. DOI: 10.1126/science.1230444.

[19] Mahreni, M., Ristianingsih, Y. (2020). A review on metal-organic framework (MOF): synthesis and solid catalyst applications. In *Proceeding of LPPM UPN "Veteran" Yogyakarta Conference Series 2020 – Engineering and Science,* 1(1), 638–645.

[20] Lee, Y.R., Jang, M.S., Cho, H.Y., Kwon, H.J., Kim, S., Ahn, W.S. (2015). ZIF-8: A comparison of synthesis methods. *Chemical Engineering Journal,* 271, 276–280. DOI: 10.1016/j.cej.2015.02.094.

[21] Butova, V., Budnyk, A., Bulanova, E.A., Lamberti, C. (2017). Hydrothermal synthesis of high surface area ZIF-8 with minimal use of TEA. *Solid State Sciences*, 69, 13–21. DOI: 10.1016/j.solidstatesciences.2017.05.002.

[22] Mohammed, W., Errayes, A. (2020). Green chemistry: principles, applications, and disadvantages. *Chemical Methodologies,* 4(4), 408–423. DOI: 10.33945/sami/chemm.2020.4.4.

[23] Glowniak, S., Szczesniak, B., Choma, J., Jaroniec, M. (2021). Mechanochemistry: toward green synthesis of metal–organic frameworks. *Materials Today,* 46, 109–124. DOI: 10.1016/j.mattod.2021.01.008.

[24] Liu, Y., Myers, E.J., Rydahl, S.A., Wang, X. (2019). ultrasonic-assisted synthesis, characterization, and application of a metal-organic framework: A green general chemistry laboratory project. *Journal of Chemical Education,* 96, 2286–2291. DOI: 10.1021/acs.jchemed.9b00267.

[25] Soni, S., Bajpai, P.K., Arora, C. (2019) A review on metal-organic frameworks: synthesis, properties, and application. *Characterization and Application of Nanomaterials,* 3(2), 1–20. DOI: 10.24294/can.v2i2.551.

[26] Adawiah, A., Oktavia, W., Saridewi, N., Azhar, F.M., Fitria, R.N., Gunawan, M.S., Komala, S., Zulys, A. (2021). Synthesis metal organic framework (MOFs) Cr-PTC-HIna modulated isonicotinic acid methylene blue photocatalytic degradation. *Bulletin of Chemical Reaction Engineering & Catalysis,* 17(2), 383–393. DOI: 10.9767/bcrec.17.2.13930.383-393.

[27] Zhong, X., Huang, C., Chen, L., Yang, Q., Huang, Y. (2022). Effect of ultrasound on the kinetics of anti-solvent crystallization of sucrose. *Ultrasonics Sonochemistry*, 82, 105886. DOI: 10.1016/j.ultsonch.2021.105886.

[28] Zhou, L., Wang, M., Yang, S., Guo, W., Pu, X., He, Y., Zhu, J., Wang, B., Zheng, M., Liu, S., Zhang, Y. (2022). Facile synthesis of mesoporous ZSM-5 aided by sonication and its application for VOCs capture. *Ultrasonics Sonochemistry*, 88, 106098. DOI: 10.1016/j.ultsonch.2022.106098.

[29] Zeiger, B.W., Suslick, K.S. (2011). Sonofragmentation of molecular crystals. *Journal of the American Chemical Society*, 133(37), 14530–14533. DOI: 10.1021/ja205867f.

[30] Pourebrahimi, S., Kazemeini, M. (2017). A kinetic study of facile fabrication of MIL-101 (Cr) metal-organic framework: effect of synthetic method. *Inorganica Chimica Acta*, 471, 513–520. DOI: 10.1016/j.ica.2017.11.033.

[31] Jankulovska, M., Berger, T., Lana-Villarreal, T., Gómez, R. (2012). A comparison of quantum-sized anatase and rutile nanowire thin films: Devising differences in the electronic structure from photoelectrochemical measurements. *Electrochimica Acta*, 62, 172–180. DOI: 10.1016/j.electacta.2011.12.016.

[32] Taheri, A., Babakhani, E.G., Towfighi, J. (2018). Study of synthesis parameters of MIL-53(Al) using experimental design methodology for CO_2/CH_4 separation. *Adsorption Science & Technology*, 36, 247–269. DOI: 10.1177/0263617416688690.

[33] Kareem, H.M., Abd Alrubaye, R.T. (2019). Synthesis and characterization of metal organic frameworks for gas storage. *IOP Conference Series: Materials Science and Engineering,* 518, 062013. DOI: 10.1088/1757-899X/518/6/062013.

[34] Ali, M.B., Maalam, K.E., Moussaoui, H.E., Mounkachi, O., Hamedoun, M., Masrour, R., Hlil, E.K., Benyoussef, A. (2015). Effect of zinc concentration on the structural and magnetic properties of mixed Co–Zn ferrites nanoparticles synthesized by sol/gel method. *Journal of Magnetism and Magnetic Materials,* 398, 20–25. DOI: 10.1016/j.jmmm.2015.08.097.

[35] Smith, J.G. (2014). *Organic Chemistry*. 4th ed. New York: McGraw-Hill.

[36] Israr, F., Chun, D., Kim, Y., Kim, D.K. (2016). High yield synthesis of Ni-BTC metal-organic framework with ultrasonic irradiation: role of polar aprotic DMF solvent. *Ultrasonics Sonochemistry,* 31, 93–101. DOI: 10.1016/j.ultsonch.2015.12.007.

[37] Zhang, B., Zhang, J., Liu, C., Sang, X., Peng, L., Ma, X., Wu, T., Hana, B., Yanga, G. (2015). Solvent determines the formation and properties of metal-organic framework. *RSC Advances,* 5, 37691–37696. DOI: 10.1039/C5RA02440D.

[38] Sharma, J., Vashishtha, M., Shah, D. (2014). Crystallite size dependence on structural parameters and photocatalytic activity of microemulsion mediated synthesized ZnO nanoparticles annealed at different temperatures. *Global Journal of Science Frontier Research*, 14(5), 19–32.

[39] Pereira, F.L., Frós, A.C.O., Amorim, M.K.M., Hallwass, F., Almeida, L.C., Barros, B.S., Kulesza, J. (2020). Ultrasound irradiation effect on morphological and adsorptive properties of a nanoscale 3D Zn-coordination polymer and derived oxide. *Ultrasonics Sonochemistry*, 69, 105275. DOI: 10.1016/j.ultsonch.2020.105275.

[40] Barros, B.S., Chojnacki, J., Soares, A.A.M., Kulesza, J., Luz, L.L., Júnior, S.A. (2015). Thermostability and photophysical properties of mixed-ligand carboxylate/benzimidazole Zn(II)-coordination polymers. *Materials Chemistry and Physics*, 162, 364–371. DOI: 10.1016/j.matchemphys.2015.05.079.

[41] Liu, H., Hou, X., Li, X., Jiang, H., Tian, Z., Ali, M.K.A. (2020). Effect of mixing temperature, ultrasonication duration and nanoparticles/surfactant concentration on the dispersion performance of Al_2O_3 nanolubricants. *Research Square*, DOI: 10.21203/rs.3.rs-84466/v1.

[42] Zarekarizi, F., Morsali, A. (2020). Ultrasonic-assisted synthesis of nano-sized metal-organic framework; a simple method to explore selective and fast congo red adsorption. *Ultrasonics Sonochemistry,* 69, 105246. DOI: 10.1016/j.ultsonch.2020.105246.

[43] Wahiduzzaman, W., Allmond, K., Stone, J., Harp, S., Mujibur, K. (2017). Synthesis and electrospraying of nanoscale MOF (metal organic framework) for high-performance CO_2 adsorption membrane. *Nanoscale Research Letters*, 12, 6. DOI: 10.1186/s11671-016-1798-6.

[44] Abbasi, A.R., Rizvandi, M. (2018). Influence of the ultrasound-assisted synthesis of Cu–BTC metal–organic frameworks nanoparticles on uptake and release properties of rifampicin. *Ultrasonics Sonochemistry,* 40, 465–71. DOI: 10.1016/j.ultsonch.2017.07.041.

[45] Nasrollahzadeh, M., Atarod, M., Sajjadi, M., Sajadi, S.M., Issabadi, Z. (2019). Plant-mediated green synthesis of nanostructures: mechanisms, characterization, and applications. *Interface Science and Technology,* 28, 199–322. DOI: 10.1016/B978-0-12-813586-0.00006-7.

[46] Yu, K., Lee, Y.R., Seo, J.Y., Baek, K.Y., Chung, Y.M., Ahn, W.S. (2021). Sonochemical synthesis of Zr-based porphyrinic MOF-525 and MOF-545: Enhancement in catalytic and adsorption properties. *Microporous and Mesoporous Materials,* 316, 110985. DOI: 10.1016/j.micromeso.2021.110985.

[47] Quan, X., Sun, Z., Meng, H., Han, Y., Wu, J., Xu, J., Xu, Y., Zhang, X. (2018). Polyethyleneimine (PEI) incorporated Cu-BTC composites: Extended applications in ultra-high efficient removal of congo red. *Journal of Solid State Chemistry,* 270, 231–241. DOI: 10.1016/j.jssc.2018.11.021.

[48] Haleem, A., Shafiq, A., Chen, S.Q., Nazar, M. (2023). A comprehensive review on adsorption, photocatalytic and chemical degradation of dyes and nitro-compounds over different kinds of porous and composite materials. *Molecules*, 28, 1081. DOI: 10.3390/molecules28031081.

[49] Blažeka, D., Car, J., Klobučar, N., Jurov, A., Zavašnik, J., Jagodar, A., Kovačević, E., Krstulović, N. (2020). Photodegradation of methylene blue and rhodamine B using laser-synthesized ZnO nanoparticles. *Materials,* 13, 4357. DOI: 10.3390/ma13194357.

[50] Kudo, A., Miseki, Y. (2009). Heterogeneous photocatalyst materials for water splitting. *Chemical Society Reviews,* 38, 253–278. DOI: 10.1039/b800489g.

[51] Xiao, J.D., Jiang, H.L. (2019). Metal-organic frameworks for photocatalysis and photothermal catalysis. *Accounts of Chemical Research,* 52, 356–366. DOI: 10.1021/acs.accounts.8b00521.